Zhongtang Huo
Jianqi Chen ✉
Lingjuan Hao
Jiansong Gao

https://doi.org/10.21278/TOF.492067624
ISSN 1333-1124
eISSN 1849-1391

A STUDY ON DYNAMIC CHARACTERISTICS OF A ROTOR SYSTEM WITH A COUPLING FAULT OF BEARING OUTER RING DEFECT AND BEARING LOOSENESS

Summary

Bearing looseness and outer ring defect occur simultaneously, affecting the dynamic characteristics of a rotor system and impeding effective health monitoring of the rotor system. Based on the theory of bearing dynamics, a model of a rotor system with a coupling fault of the outer ring defect and bearing looseness was established. The vibration response was obtained through numerical simulation, and the effect of rotational speed on the vibration characteristics of the system was also discussed. The results showed that $f_r/2$ and its harmonics appeared in the frequency spectrum of the bearing with both looseness and an outer ring defect and their amplitudes were proportional to the rotational speed. In addition, the combined frequency of $f_r/2$ and the outer ring defect frequency f_o can be considered as the frequency of the coupling fault, which was also reflected in the other bearing of the rotor system. The research results provide ideas for fault monitoring of the rotor system with a coupling fault of bearing looseness and outer ring defect.

Key words: *looseness, outer ring defect, coupling, dynamic model, fault diagnosis*

1. Introduction

Following the development of the manufacturing industry, bearing rotor systems have been widely used in aerospace, electric power systems, transportation, and precision machining [1-4]. Manufacturing errors, assembly precision, and long-term machine overloading inevitably lead to the loosening of system bearings, and the coupling failure of the outer ring occurs. This in turn leads to system shutdown, resulting in significant economic losses and even casualties. Therefore, the study of dynamic characteristics of the rotor system under the joint action of bearing loosening and bearing outer ring defect is of great significance for the design, installation, and fault diagnosis of the rotor system.

Being an important part of rotating equipment, the running state and fault diagnosis of bearing rotor systems have always been the key research topic [5-8]. The dynamic model is an effective method for exploring the mechanism of changes in the dynamic characteristics of a bearing rotor system and it is also an important method for obtaining various bearing fault characteristics [9, 10]. Based on the bearing fault dynamics theory, Liu et al. [11] established a

crack failure model of the bearing outer ring and studied the dynamic response of the bearing outer ring crack. Wang et al. [12] established a rotor coupling dynamic model considering the interaction between the bearing outer ring and the support and analysed the response characteristics of the bearing and the rotor considering the fault of looseness. Duan et al. [13] predicted the dynamic response of gear crack evolution by calculating the model of a coupling system of shell, bearing, shaft, and gear, and verified the validity of the proposed method through simulation and experiment. Dai et al. [14] established a coupled system dynamics model of local spalling of a bearing and fault of a gear pair and studied the change pattern of system stiffness.

In addition, the characteristics of looseness vibration in the rotor system, as a common scenario in production practice, have been a focus of scholarly research. Cao et al. [15] proposed that the bearing loosening was caused by the clearance fit between the outer ring and the bearing seat and studied the effect of this non-linearity of the clearance on the nonlinear vibration of the system. Bai et al. [16, 17] considered the temperature variation gap caused by the thermal deformation difference between ceramic bearings and steel seats, investigated the influence of temperature on the dynamic response of the rotating subsystem through experiments, and obtained the vibration characteristics of the system when the bearing was loose. Wang et al [18] developed a dynamic model of a bearing-coupling-rotor system and analysed the bearing vibration response under misalignment conditions. Nan et al. [19] formulated a dynamic model of a rotor system with bolt looseness and impact-rub coupling, investigating the influence mechanisms of eccentricity, disk spacing, and looseness clearance on rotor dynamics. The above studies did not consider the more common bearing defects in practice and could not obtain the vibration characteristics of bearing outer ring defect and bearing looseness coupling. However, the above research results provide a certain reference for this paper's research ideas and methods. Based on the previous scholars' research on the coupling fault of the rotating subsystem, this paper establishes a dynamic model of the bearing outer ring defect and bearing looseness coupling, analyses the rotor system vibration dynamic characteristics of a bearing with outer ring defects and looseness, obtains the dynamic vibration characteristics of two bearings in the rotor system containing the above-mentioned coupling fault, and provides a theoretical basis for the diagnosis of bearing rotor system faults. Section 2 introduces a dynamic model of the rotor system with a coupling fault attributed to loose outer ring defects. In Section 3, numerical simulation analyses are conducted to investigate the dynamic behaviour of the rotor system. Section 4 validates the accuracy of the proposed method through experiments conducted on a bearing failure test bench. These experiments serve as an essential theoretical foundation for understanding the characteristics of the coupling fault in bearing rotor systems. Finally, Section 5 summarises the main conclusions drawn from this investigation.

2. Dynamic model of bearing looseness and outer ring defects

2.1 Force analysis of bearings

Firstly, a geometric model of a bearing rotor system was established as shown in Fig. 1. In this model, the bearing with a mass of m_{rL} on the left end of the system disengages from the bearing housing, resulting in a loosening fault with a loosening gap of δ_a. Meanwhile, there is a local defect on the outer ring raceway of the bearing. The identical bearing on the right end of the system is healthy.

Coordinate systems $[O_{rL},Y_{rL},Z_{rL}]$ and $[O_{rR},Y_{rR},Z_{rR}]$ were established to quantify the motion behaviour of bearings. After the bearing vibration occurs, the motion coordinate systems of the two bearings deviate from their respective fixed coordinate systems $[O_L,Y_L,Z_L]$ and $[O_R,Y_R,Z_R]$. Assuming that the geometric centres of the bearings and the bearing housing coincide at the initial moment, they move along their respective motion coordinate systems $[O_{rL},Y_{rL},Z_{rL}]$ and $[O_{rR},Y_{rR},Z_{rR}]$, and according to the concentrated mass method, it is assumed that the mass of the shaft is concentrated in the middle disk with a mass of m_{rp}.

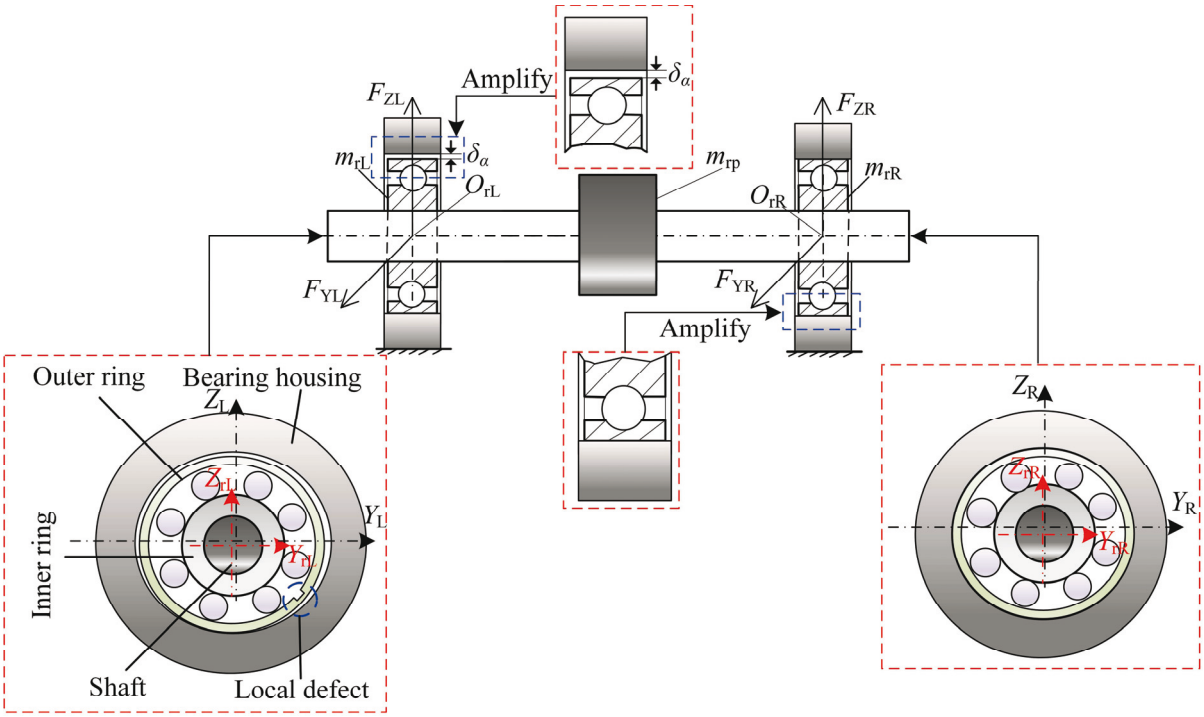

Fig. 1 Bearing rotor system with coupling fault of bearing looseness and outer ring defect

When the rotor system works, the two bearings vibrate in their respective motion coordinate systems. Assuming that the outer ring is fixed at the initial moment, the inner ring and the shaft are fixed together and rotate with the shaft. Moreover, the mass of the inner ring and the shaft relative to the outer ring is large, so the motion of the bearing can be regarded as the vibration of the outer ring relative to the inner ring. When the outer ring moves y and z relative to the inner ring along the $Y_{rL(rR)}$ and $Z_{rL(rR)}$ axes, the total deformation of the jth rolling element in contact with the inner and outer rings at a certain moment is:

$$\delta_j = y_{rL(rR)} \cos\varphi_j + z_{rL(rR)} \sin\varphi_j - \mu \tag{1}$$

where μ represents the radial clearance inside the bearing, (y_{rL}, z_{rL}) and (y_{rR}, z_{rR}) represent the displacement of the bearings at the left and right end of the system in their respective coordinate systems, and φ_j denotes the angular position of the jth rolling element as shown in Fig. 2, which can be also represented in Eq. (2). In addition, in Fig. 2, the diameter of the inner raceway of the bearing is d_i, assuming that the distance between the centre of mass and geometric centre of the bearing fixed to the shaft is e, the angular velocity of the shaft is ω, and the angle between the coordinate systems [O_{rL},Y_{rL},Z_{rL}] and [O_L,Y_L,Z_L] is ωt.

$$\varphi_j = \frac{2\pi}{N_b}(j-1) + \omega_c t \tag{2}$$

where N_b is the total number of rolling elements, d_b is used to represent the diameter of the rolling element, and d_m is used to represent the pitch diameter of the ball bearing, and ω_c is the angular velocity of the rotational speed of the rolling elements, which can be expressed as:

$$\omega_c = \frac{1}{2}\left(1 - \frac{d_b}{d_m}\right)\frac{2\pi n}{60} \tag{3}$$

where n is the input speed of the rotor system.

According to the Hertz contact theory [20-21], the equivalent pressure exerted by the jth rolling element on the inner and outer races of the bearing is:

$$Q_j = K\delta_j^{3/2} \tag{4}$$

where K represents the equivalent contact stiffness [22]. Thus, the bearing force of the rolling bearing is:

$$\begin{aligned} F_{\mathrm{YL(YR)}} &= \sum_{j=1}^{N_\mathrm{b}} Q_j \cdot \cos\varphi_j \\ F_{\mathrm{ZL(ZR)}} &= \sum_{j=1}^{N_\mathrm{b}} Q_j \cdot \sin\varphi_j \end{aligned} \tag{5}$$

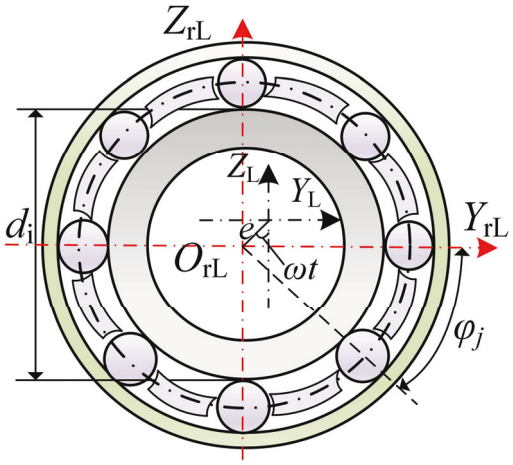

Fig. 2 Bearing model

2.2 Initial analysis of the outer ring defect

When a single defect exists on the outer race of the left bearing presented in Fig. 1, the rolling element will undergo additional deformation as it passes through the defective area, as illustrated in Fig. 3, and can be expressed as:

$$\delta'_j = y_{\mathrm{rL}}\cos\varphi_j + z_{\mathrm{rL}}\sin\varphi_j - \mu - \beta\cdot\lambda \tag{6}$$

where λ is the amount of deformation released when the rolling body passes through the defective region, which can be expressed as:

$$\lambda = \begin{cases} O_\mathrm{d} & O_\mathrm{d} < \lambda_{\max} \\ \dfrac{d_\mathrm{b}}{2} - \sqrt{\left(\dfrac{d_\mathrm{b}}{2}\right)^2 - \left(\dfrac{l}{2}\right)^2} & O_\mathrm{d} \geq \lambda_{\max} \end{cases} \tag{7}$$

where O_d is the defect depth and l is the defect width. Considering the position angle ϕ_{do} and the opening angle $\Delta\phi_{\mathrm{do}}$ of the defect, the switching quantity β can be expressed as:

$$\beta = \begin{cases} 1 & 2n_j\pi + \varphi_{\mathrm{do}} \leq \varphi_j \leq 2n_j\pi + \varphi_{\mathrm{do}} + \Delta\varphi_{\mathrm{do}} \\ 0 & \text{else} \end{cases} \tag{8}$$

where n_j is the number of rolling body revolutions and can be expressed as:

$$n_j = \begin{cases} \mathrm{int}\left(\dfrac{\omega_\mathrm{c} t}{2\pi}\right) & \varphi_{\mathrm{do}} \geq \dfrac{2\pi(j-1)}{N_\mathrm{b}} \\ \mathrm{int}\left(\dfrac{\omega_\mathrm{c} t}{2\pi}\right) + 1 & \varphi_{\mathrm{do}} \leq \dfrac{2\pi(j-1)}{N_\mathrm{b}} \end{cases} \tag{9}$$

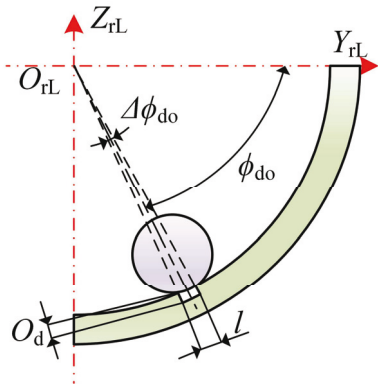

Fig. 3 Outer ring defect model

2.3 Analysis of the loose bearing force

When the left bearing from Fig 1. is loose, it will come in contact with the housing as shown in Fig. 4, and according to Hooke's law, the collision force F_p between the loose bearing and the housing can be expressed as:

$$F_p = k\left(\sqrt{y_{rL}^2 + z_{rL}^2} - \frac{\delta_\alpha}{2}\right) \tag{10}$$

However, this collision force is only generated when the bearing comes in contact with the bearing housing under the following conditions:

$$\sqrt{y_{rL}^2 + z_{rL}^2} - \frac{\delta_\alpha}{2} \geq 0 \tag{11}$$

where k represents the contact stiffness between the bearing and the housing, δ_a is the bearing looseness clearance, and F_f is the Coulomb friction, which can be expressed as:

$$F_f = \mu_f F_p \tag{12}$$

where u_f is the friction coefficient between the bearing and the bearing housing, taken as 0.2 [17].

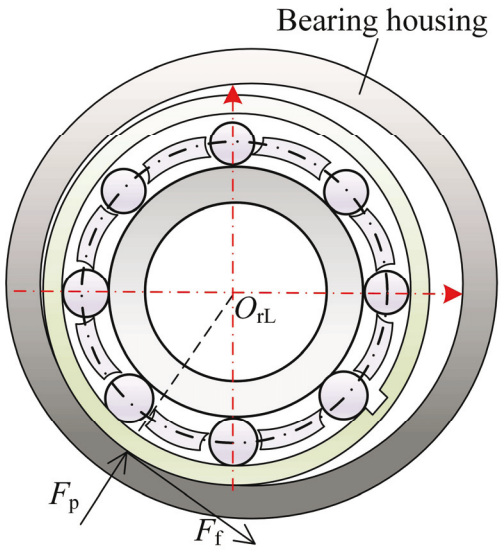

Fig. 4 Bearing loosening model

2.4 Development of a dynamic model of the rotor system with an outer ring defect and bearing looseness

Figs. 5-7 show the three parts of the rotor system presented in Fig. 1 according to the allocation principle of the centralized mass method. Fig. 5 shows the bearing with a coupling fault on the left end of the system, Fig. 6 shows the mechanical analysis of the rotor set based on the centralized mass method, and Fig. 7 shows the mechanical analysis of the healthy bearing on the right end of the system.

Firstly, since the axis is an elastic axis, it is assumed that the initial vibration of the two bearings is oriented in the positive direction of the coordinate axis. Due to the connection effect of the elastic shaft, the elastic forces between the defective bearing and the rotor in different directions are $k_Z(z_{rL}\text{-}z_{rp})$ and $k_Y(y_{rL}\text{-}y_{rp})$, respectively. In addition, due to the shaft being fixed together with the inner ring of the bearing and rotating synchronously, the defective bearing is subjected to an eccentric force. In this bearing, the sum of the contact forces between each rolling element and the inner ring constitutes the bearing forces F_{YL} and F_{ZL}, and the loosening of the bearing and the bearing housing will generate F_p and F_f.

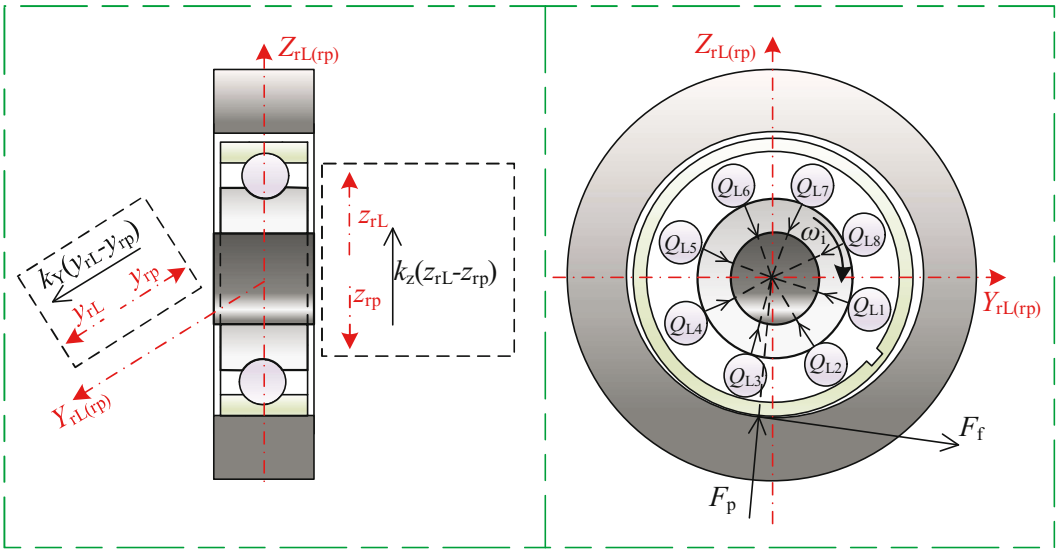

Fig. 5 Mechanical analysis of the bearing with a coupling fault on the left end of the system

Fig. 6 shows the mechanical analysis of the rotor set based on the centralized mass method. Due to the assumption that the mass of the shaft is concentrated on the rotor disc, the rotor is subjected to elastic forces transmitted through the elastic shaft from both bearings, but the direction of the force is opposite to that acting on the bearings, as shown in Fig. 6. In addition, due to the rotation of the shaft, the rotor is subjected to an eccentric force, which is reflected in two directions.

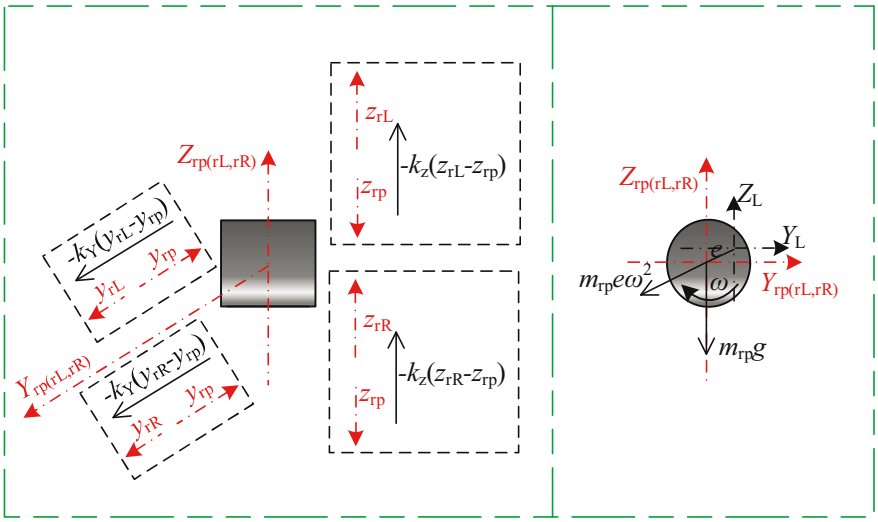

Fig. 6 Mechanical analysis of rotor

Fig. 7 shows the mechanical analysis of the healthy bearing on the right end of the system. The force borne by the bearing is basically the same as that of the defective bearing, but this bearing is healthy, so it is not in contact with the bearing housing and there is no additional fault excitation due to local defects. As shown in Fig. 7, the bearing is subjected to an elastic force from the elastic shaft, its own bearing force, and the eccentric force generated by rotation.

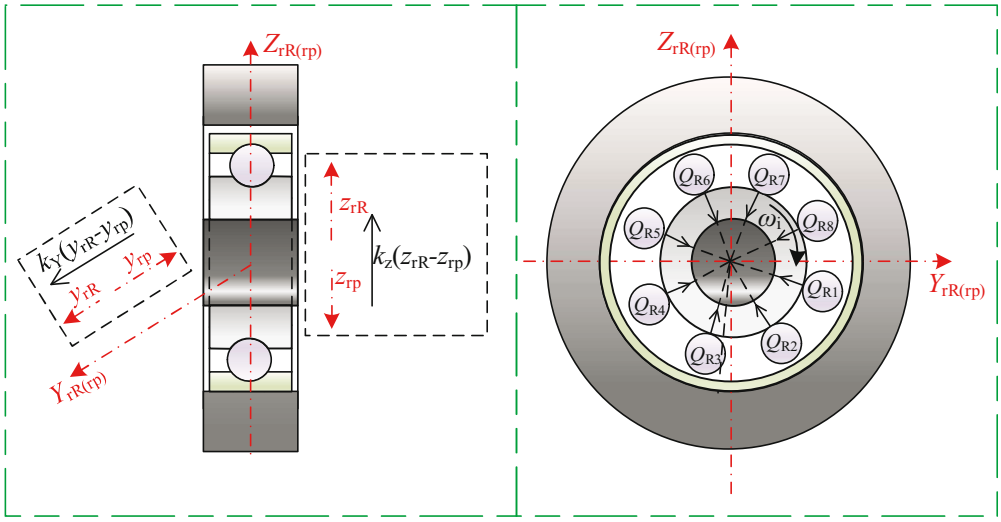

Fig. 7 Mechanical analysis of the healthy bearing on the right end of the system

Combining Fig. 1, Fig. 5, Fig. 6, and Fig. 7, the dynamic equation system of the bearing rotor system can be expressed as [23]:

$$\begin{cases} m_{rp}\ddot{y}_{rp}+c_{rp}\dot{y}_{rp}+k_Y\left(y_{rp}-y_{rR}\right)+k_Y\left(y_{rp}-y_{rL}\right)=m_{rp}e\omega^2\cos(\omega t) \\ m_{rp}\ddot{z}_{rp}+c_{rp}\dot{z}_{rp}+k_Z\left(z_{rp}-z_{rR}\right)+k_Z\left(z_{rp}-z_{rL}\right)=m_{rp}e\omega^2\sin(\omega t)-m_{rp}g \\ m_{rR}\ddot{y}_{rR}+c_{rb}\dot{y}_{rR}+k_Y\left(y_{rR}-y_{rp}\right)-m_{rR}e\omega^2\cos(\omega t)=F_{YR} \\ m_{rR}\ddot{z}_{rR}+c_{rb}\dot{z}_{rR}+k_Z\left(z_{rR}-z_{rp}\right)-m_{rR}e\omega^2\sin(\omega t)=F_{ZR}-m_{rR}g \\ m_{rL}\ddot{y}_{rL}+c_{rb}\dot{y}_{rL}+k_Y\left(y_{rL}-y_{rp}\right)+F_p\cos(\omega t)+F_f\sin(\omega t)-m_{rL}e\omega^2\cos(\omega t)=F_{YL} \\ m_{rL}\ddot{z}_{rL}+c_{rb}\dot{z}_{rL}+k_Z\left(z_{rL}-z_{rp}\right)+F_p\sin(\omega t)+F_f\cos(\omega t)-m_{rL}e\omega^2\sin(\omega t)=F_{ZL}-m_{rL}g \end{cases} \tag{13}$$

where m_{rp} is the rotor mass, e is the rotor eccentricity, ω is the input angular velocity of the rotor system, and m_{rL}, m_{rR} are the defective and healthy bearing masses, respectively.

3. Simulation calculation

The type of the bearing rotor system selected for the calculation is JIS 6306 [23] and the dimensional parameters are given in Table 1. The rotor system operates at an input speed of 600 r/min, the equivalent contact stiffness K value is 7e+10, c_{rp}=2100 N·s/m, rotor eccentricity e=0.01 mm, O_d =0.1 mm, l=3 mm, and the friction coefficient between the bearing and the bearing housing is 0.1. The amount of looseness δ_α=0.03 mm and the mass of the rotor disc is about 11 kg. The time step for the simulation calculation is 10^{-5}, neglecting the sliding effect of the bearing. The frequency of the outer ring defect of the bearing is:

$$f_o = \frac{f_r}{2}\left(1-\frac{d_b}{d_m}\right)N_b = 30.8\text{Hz} \tag{14}$$

Table 1 Bearing parameters

Parameters	Numerical values
Inner ring diameter d_i (mm)	40.1
Outer ring diameter d_o (mm)	63.9
Rolling body diameter d_b (mm)	11.9
Number of rolling elements N_b	8
Bearing clearance μ (mm)	0.04
Contact stiffness k (N/m)	2.5×10^7
Damping factor c_{rb} (N·s/m)	200

Through the numerical simulation, vibration waveforms of the bearing with a coupling fault were obtained, as shown in Fig. 8. The time interval Δt between the adjacent peaks in the time domain waveforms of directions y and z in Fig. 8 is approximately 0.33 s. According to the rolling bearing order analysis method, it is approximately equal to $1/f_o$, which is consistent with the result obtained from Eq. 14, validating the correctness of the model. This confirms that the simulation results are typical of the dynamic model of bearings with an outer ring fault.

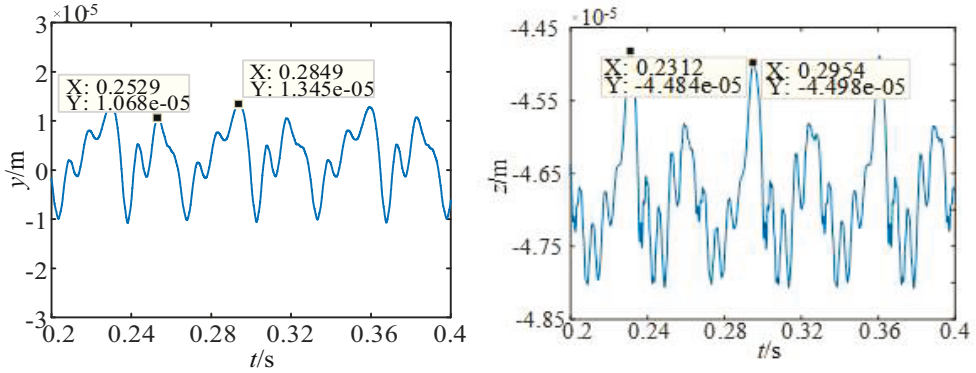

Fig. 8 Time domain diagram of simulation of bearing with a coupling fault

The simulation results were subjected to the Fast Fourier Transform (FFT) to obtain the spectrum shown in Fig. 9. The spectrum exhibits the presence of $f_r/2$ and its harmonics, f_r and its harmonics, f_o, as well as combination frequencies of $f_r/2$ and its harmonics with f_o, evident in both y and z directions. The presence of $f_r/2$ and its harmonics components is characteristic

of dry frictional rubbing, indicative of loose elements in the rotor system in addition to basic looseness and other dry friction characteristics. This occurrence aligns with the findings of Bai [16]. Additionally, the appearance of the outer ring defect frequency f_o in the spectrum indicates the presence of an outer ring defect. The combination frequencies of $f_r/2$ and its harmonics with f_o reflect the existence of the coupling fault of bearing looseness and outer ring defect.

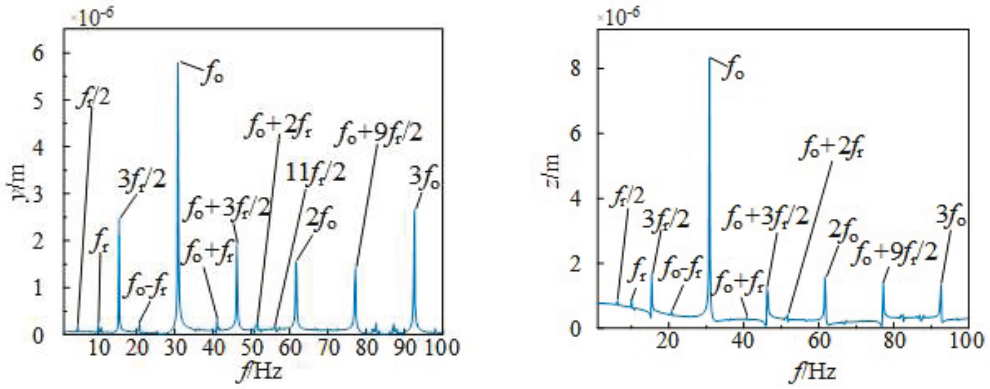

(a) **(b)**

Fig. 9 Vibration spectrum of defective bearing at 600 r/min

The vibration spectrum of the defective bearing with a coupling fault was obtained by varying the input speed, as depicted in Fig. 10. As the speed increases, the eccentric excitation becomes positively correlated with the speed, leading to successive increases in the amplitude of f_r, as shown in Figs. 10 and11. Moreover, the higher speed results in increased vibration of the loose bearing and intensified rubbing between the bearing and its seat, causing an increase in the amplitude of $f_r/2$ and its harmonics. The characteristic of the fault of looseness is amplified, eventually making $f_r/2$ and its harmonics the predominant components in the spectrum. Additionally, the combination frequency components of $f_r/2$ and its harmonics with f_o persist, indicating that the speed does not alter the fault characteristics of the coupling fault. The characteristics of the coupling fault related to the frequencies of looseness and the outer ring defect remain the predominant frequency components in the spectrum.

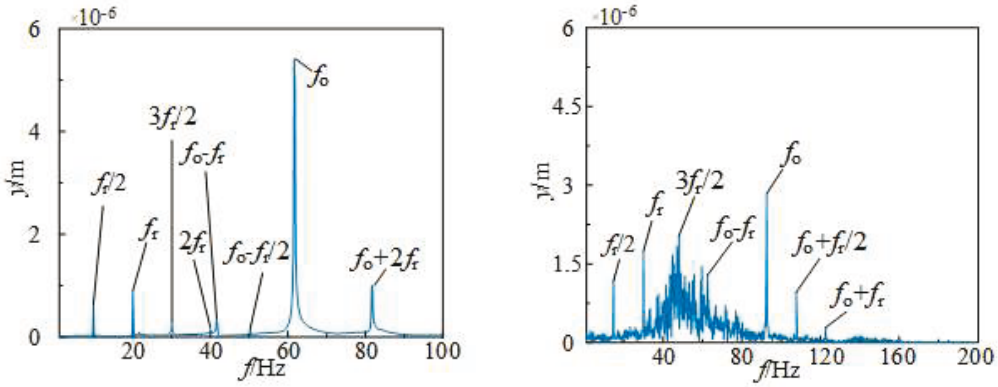

(a) 1,200 r/min **(b)** 1,800 r/min

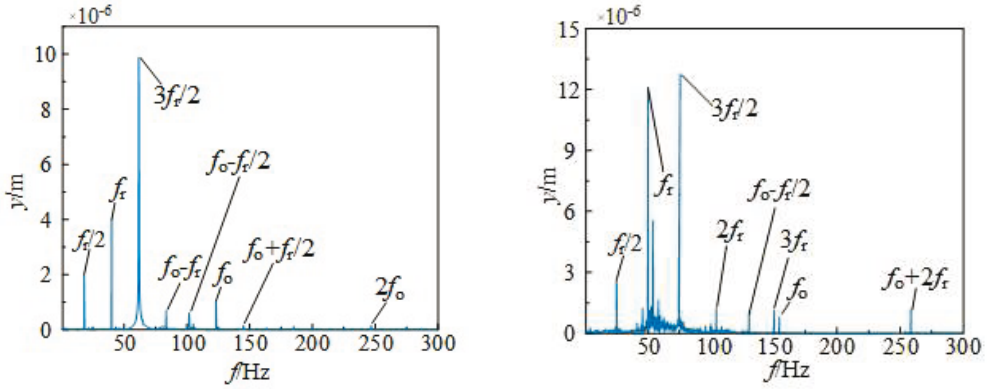

(c) 2,400 r/min **(d)** 3,000 r/min

Fig. 10 Vibration spectra of the defective bearing at 1,200 r/min, 1,800 r/min, 2,400 r/min, and 3,000 r/min

Fig. 11 shows the trend of the frequency components from Fig. 10 at different rotational speeds. In Fig. 11, it can be found that the periodic impact vibration induced by the outer ring defect causes a significant amplitude increase in f_r. Also, as the rotational speed rises, the intensified collision forces caused by bearing looseness partially counteract the fault excitation, leading to a reduction in the amplitude of f_o.

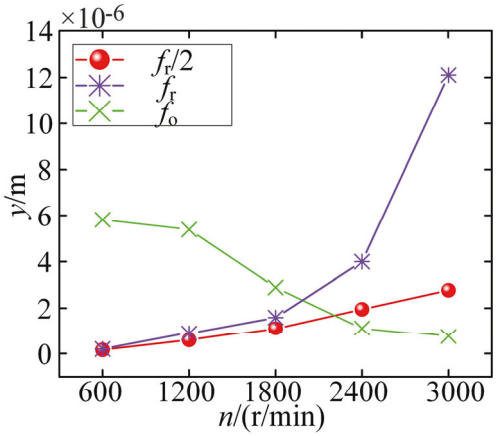

Fig. 11 Trend of frequency amplitude

Fig. 12 shows the vibration spectrum of the healthy bearing at the right end of the rotor system. Compared to the spectrum of the bearing with a coupling fault at the left end of the system, at lower speeds, f_r and its harmonics, as well as the combination frequencies of f_r and its harmonics with f_o, are the predominant frequency components. There are no components of $f_r/2$ and its harmonics or combination frequencies in the spectrum. However, a faint outer ring defect frequency f_o can be observed, and its amplitude does not show significant changes with speed variations, indicating that the bearing has not experienced an outer ring defect. The outer ring defect frequency characteristic f_o is transmitted to this bearing from the opposite end of the rotor system [24, 25]. As the speed increases, the components of $f_r/2$ and its harmonics, as well as the combination frequencies of $f_r/2$ and its harmonics with f_o, gradually appear in the spectrum, but their amplitudes remain weak and are significantly influenced by the speed. Their amplitudes always remain lower than those of f_r and its harmonics, indicating that the fault of looseness of the defective bearing is transmitted to the healthy bearing at the right end of the system. Additionally, the presence of $2f_r$, $3f_r$, etc., in the spectrum indicates misalignment between the two bearings in the rotor system, which is consistent with the findings of Bai [17].

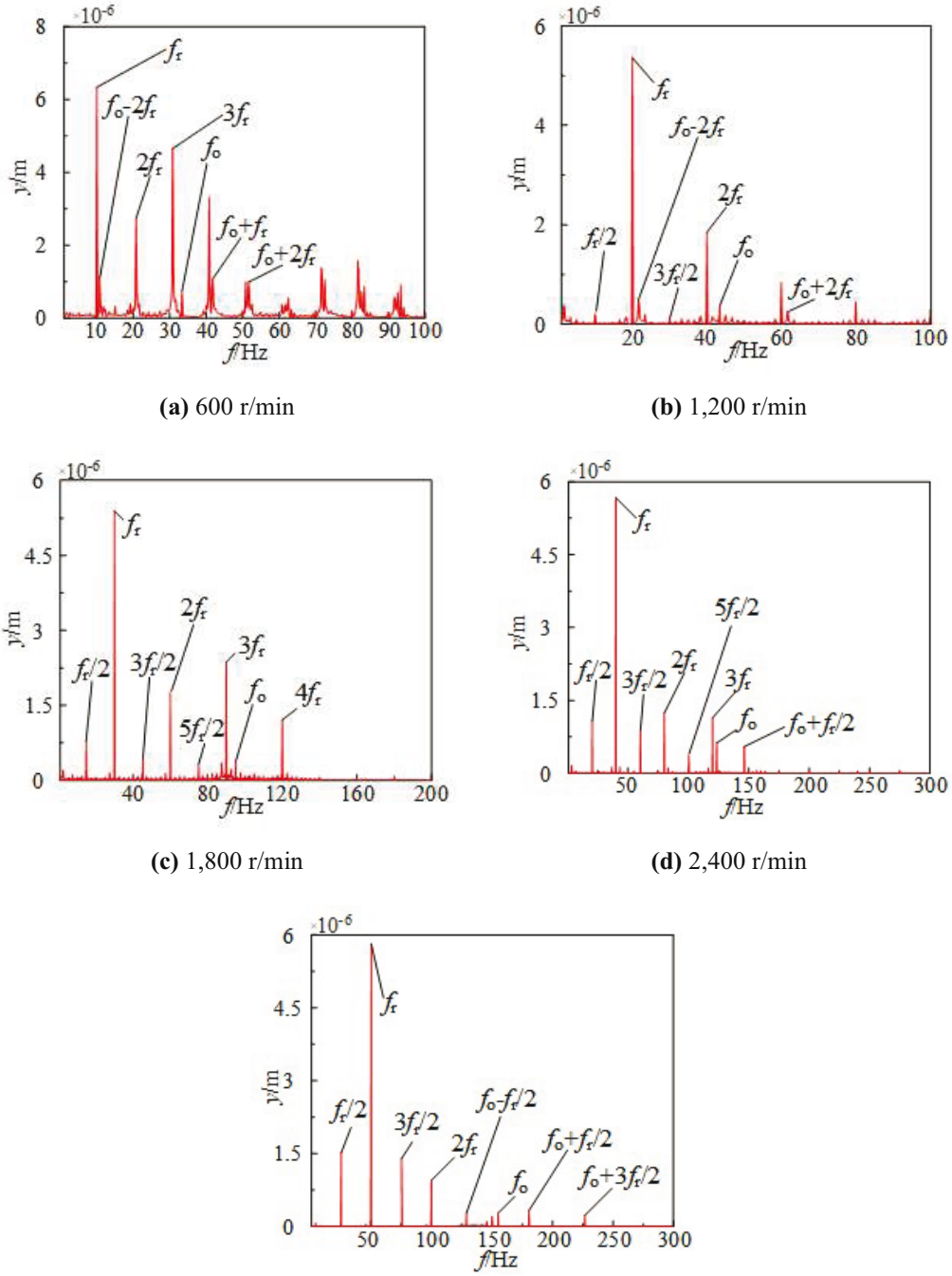

(a) 600 r/min

(b) 1,200 r/min

(c) 1,800 r/min

(d) 2,400 r/min

(e) 3,000 r/min

Fig. 12 Vibration spectra of healthy bearing at 600 r/min, 1,200 r/min, 1,800 r/min, 2,400 r/min, and 3,000 r/min

4. Experimental verification

In this section, a dynamic model of the bearing rotor system with a coupling fault of an outer ring defect and bearing looseness was validated through simulated experiments on a bearing fault simulation test rig, as shown in Fig. 13. The motor output speed range of 0-10,000 r/min and stable speed can be controlled by a speed controller through the coupling to drive the shaft and the rotation of the two bearing inner rings. In the bearing rotor system, the bearing at the left end near the motor is a bearing with an outer ring defect, and the defect size is consistent with the machining in the simulation calculation. In addition, the physical and structural parameters of the two bearings on the rotor system are completely consistent with

those used in the simulation, thus ensuring the accuracy of the experimental testing. To simulate the loosening of this bearing, the bearing housing hole was machine finished by sandpaper grinding, during which the circumferential dimensions were measured several times using Vernier calipers and roundness gauges so that the clearance between the bearing and the housing was 0.03 mm and the roundness of the bearing hole was ensured to be good. Vibration signals were collected using contact displacement sensors at a sampling frequency of 1,024 Hz and collected by a data acquisition device.

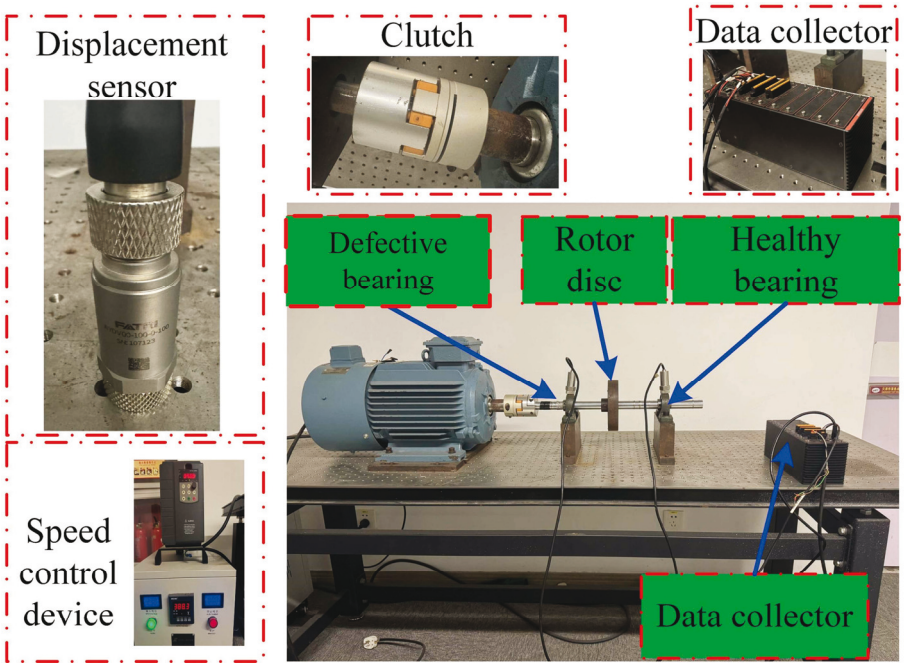

Fig. 13 Experimental system of defective bearing

Firstly, the input speed was set to 600 r/min and vibration signals from both bearings were collected and subjected to the FFT to obtain the spectra of the two bearings as depicted in Fig. 14. Since the defective bearing has both looseness and an outer ring defect, the spectrum exhibits components of $f_r/2$ and its harmonics, as well as the combination frequency components of $f_r/2$ and its harmonics with f_o. Additionally, because both bearings were arranged on the same shaft, the healthy bearing at the right end of the system shows faint frequency components of f_o, as well as combination frequency components of f_r and its harmonics with f_o. This is consistent with the results of the simulation calculations, validating also the correctness of the model.

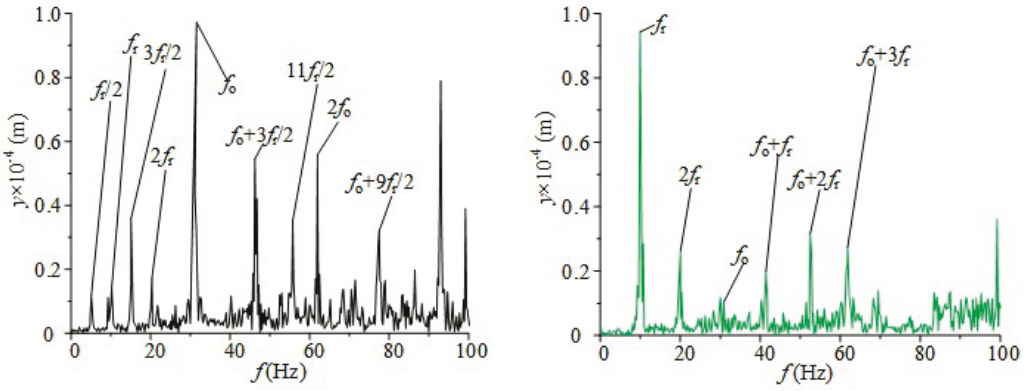

(a) Vibration spectrum of defective bearing **(b)** Vibration spectrum of healthy bearing

Fig. 14 Vibration spectra of two bearings

The rotational speed controller was adjusted so that the rotational speeds were 1,200 r/min, 1,800 r/min, 2,400 r/min, and 3,000 r/min and the vibration spectra of the two bearings were obtained as depicted in Figs. 15-18. As the speed increases, the spectrum of the defective bearing gradually shows that components of $f_r/2$ and its harmonics replace f_r and its harmonics as the predominant frequency components. Additionally, f_o remains present throughout, indicating the continuous presence of the outer ring defect frequency. However, due to the greater influence of the increased speed on f_r and its harmonics as well as $f_r/2$ and its harmonics, compared to f_o, the modulation amplitude of f_o is slightly reduced. Meanwhile, the combination frequency components of $f_r/2$ and its harmonics with f_o emerge as the speed increases, indicating the presence of the coupling fault, which is consistent with the simulation calculations and validates the correctness of the model.

Furthermore, the spectrum of the healthy bearing at the right end of the system exhibits significant components of f_r and its harmonics, strongly correlated with the speed. At higher speeds, it also shows fault characteristics of looseness and defect characteristics transmitted from the defective bearing. However, the components of f_r and its harmonics remain the predominant frequency components in the spectrum, indicating the health of this bearing and validating the model.

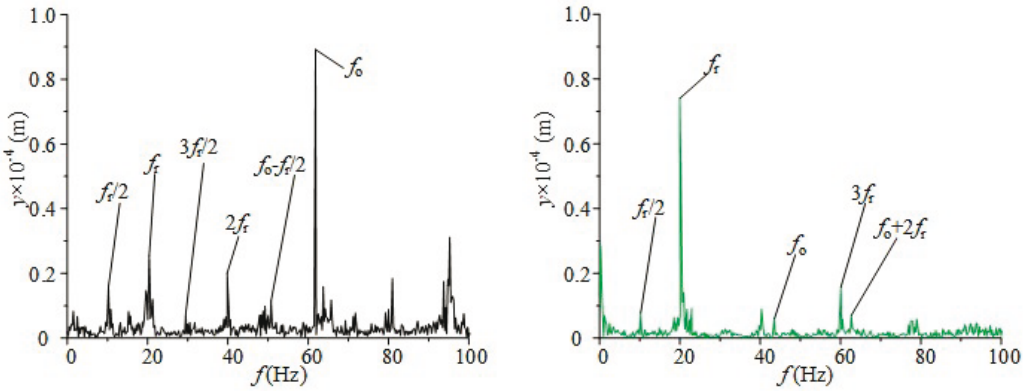

(a) Vibration spectrum of defective bearing **(b)** Vibration spectrum of healthy bearing

Fig. 15 Vibration spectra of two bearings at 1,200 r/min

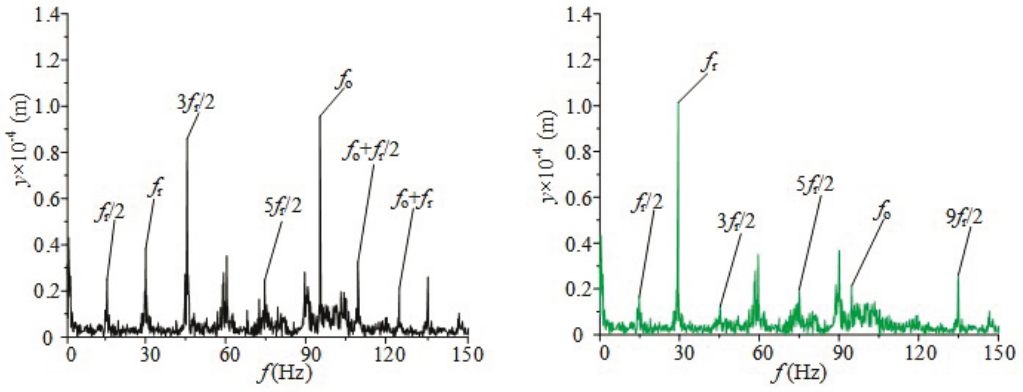

(a) Vibration spectrum of defective bearing **(b)** Vibration spectrum of healthy bearing

Fig. 16 Vibration spectra of two bearings at 1,800 r/min

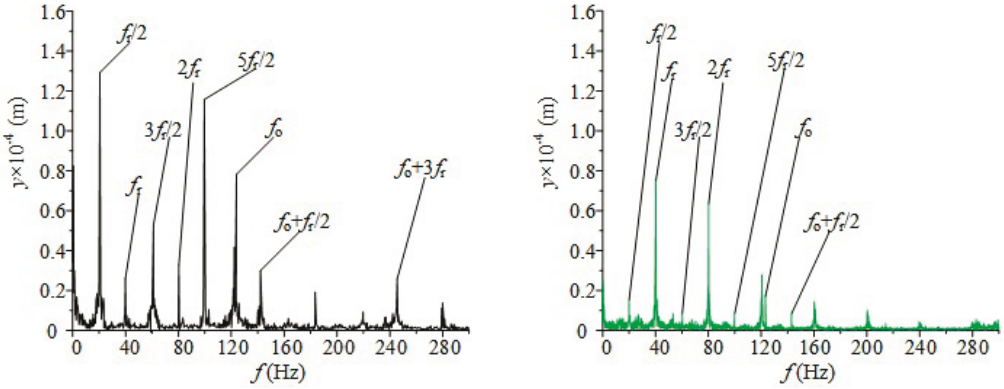

(a) Vibration spectrum of defective bearing **(b)** Vibration spectrum of healthy bearing

Fig. 17 Vibration spectra of two bearings at 2,400 r/min

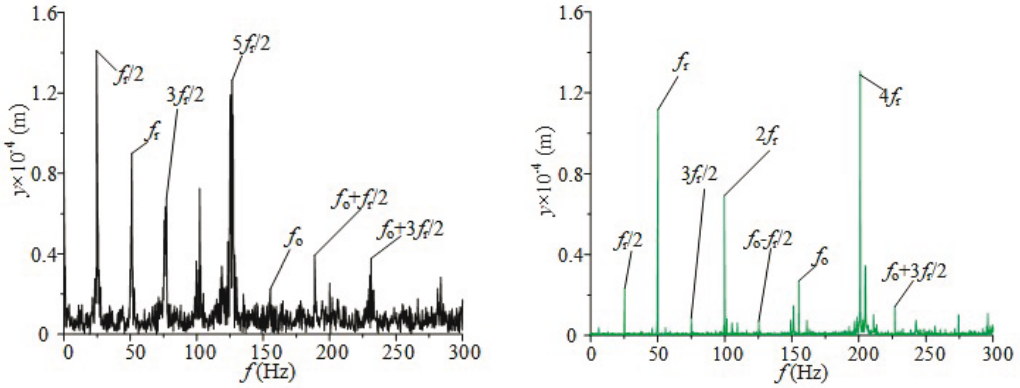

(a) Vibration spectrum of defective bearing **(b)** Vibration spectrum of healthy bearing

Fig. 18 Vibration spectra of two bearings at 3,000 r/min

5. Conclusion

Considering the scenario of a rotor system in which one end of the bearing is the loose and defective outer ring and the other end is healthy, a dynamic model of the rotor system was developed based on the concentrated mass method and then verified with the help of experimental means. The main conclusions of the study are as follows:

(1) The bearing faults of bearing looseness and the bearing outer ring defect are obvious, mainly manifested in the presence of $f_r/2$ and its octave components on the frequency spectrum, $f_r/2$ and its octave, and f_o combination of frequency components.

(2) The coupling fault characteristics of the bearing looseness and the bearing outer ring defect are enhanced when the speed is increased. The combination frequency of $f_r/2$, its octave, and f_o gradually became the most dominant frequency component in the frequency spectrum.

(3) The healthy bearing of the rotor system, connected by the shaft, shows enhanced frequency components associated with looseness as the speed varies. The frequency components related to the outer ring defect are not strongly correlated with the speed. However, the predominant frequency components in the spectrum are always f_r and its harmonics. This can serve as a reference for monitoring multi-bearing rotor systems.

REFERENCES

[1] Shi H, Bai X, Zhang K, et al. Effect of thermal-related fit clearance between outer ring and pedestal on the vibration of full ceramic ball bearing. Shock and Vibration, 2019, 2019: 8357807. https://doi.org/10.1155/2019/8357807

[2] Shinde P V, Desavale R G, Jadhav P M, et al. A multi fault classification in a rotor-bearing system using machine learning approach. Journal of the Brazilian Society of Mechanical Sciences and Engineering, 2023, 45(2): 121. https://doi.org/10.1007/s40430-023-04015-1

[3] Tian M, Su X, Chen C, et al. Bearing fault diagnosis of wind turbines based on dynamic multi-adversarial adaptive network. Journal of Mechanical Science and Technology, 2023, 37(4): 1637-1651. https://doi.org/10.1007/s12206-023-0306-z

[4] Wang C, Tian J, Zhang F, et al. Dynamic modeling and simulation analysis of inter-shaft bearing fault of a dual-rotor system. Mechanical Systems and Signal Processing, 2023, 193 https://doi.org/10.1016/j.ymssp.2023.110260

[5] Liu J, Tang C, Pan G. Dynamic modeling and simulation of a flexible-rotor ball bearing system. Journal of Vibration and Control, 2022, 28(23-24): 3495-3509. https://doi.org/10.1177/10775463211034347

[6] Ma S, Yin Y, Chao B, et al. A real-time coupling model of bearing-rotor system based on semi-flexible body element. International Journal of Mechanical Sciences, 2023, 245. https://doi.org/10.1016/j.ijmecsci.2022.108098

[7] Yang R, Zhang Z, Chen Y. Analysis of vibration signals for a ball bearing-rotor system with raceway local defects and rotor eccentricity. Mechanism and Machine Theory, 2022, 169. https://doi.org/10.1016/j.mechmachtheory.2021.104594

[8] Zhang J, Han D, Xie Z, et al. Nonlinear behaviors analysis of high-speed rotor system supported by aerostatic bearings. Tribology International, 2022, 170. https://doi.org/10.1016/j.triboint.2021.107111

[9] Xu H, Wang P, Ma H, et al. Analysis of axial and overturning ultimate load-bearing capacities of deep groove ball bearings under combined loads and arbitrary rotation speed. Mechanism and Machine Theory, 2022, 169. https://doi.org/10.1016/j.mechmachtheory.2021.104665

[10] Hemati A, Shooshtari A. Bearing Failure Analysis Using Vibration Analysis and Natural Frequency Excitation. Journal of Failure Analysis and Prevention, 2023, 23(4): 1431-1437. https://doi.org/10.1007/s11668-023-01700-0

[11] Liu Z M, Bai X T, Shi H T, et al. A recognition method for crack position on the outer ring of full ceramic bearing based on the synchronous root mean square difference. Journal of Sound and Vibration, 2021, 515. https://doi.org/10.1016/j.jsv.2021.116493

[12] Wang H, Guan X, Chen G, et al. Characteristics analysis of rotor-rolling bearing coupled system with fit looseness fault and its verification. Journal of Mechanical Science and Technology, 2019, 33: 29-40. https://doi.org/10.1007/s12206-018-1204-7

[13] Duan T, Wei J, Yan Q, et al. Detecting the 3D spatial varying crack evolution-induced vibration of gearbox through a system level rigid-flexible coupling model. Mechanism and Machine Theory, 2022, 174. https://doi.org/10.1016/j.mechmachtheory.2022.104892

[14] Dai P, Wang J, Yan S, et al. Effects of localized defects of gear-shaft-bearing coupling system on the meshing stiffness of gear pairs. Journal of Vibration Engineering & Technologies, 2022, 10(3): 1153-1173. https://doi.org/10.1007/s42417-022-00435-w

[15] Cao H, Shi F, Li Y, et al. Vibration and stability analysis of rotor-bearing-pedestal system due to clearance fit. Mechanical Systems and Signal Processing, 2019, 133. https://doi.org/10.1016/j.ymssp.2019.106275

[16] Bai X, Sun M, Wang Z, et al. Loose Coupling Mechanism and Fault Characteristics Analysis of Multiple Connections in Full Ceramic Bearing-Pedestal-Foundation System Within Wide Temperature Ranges. Journal of Failure Analysis and Prevention, 2024: 1-13. https://doi.org/10.1007/s11668-024-01862-5

[17] Bai X, Zheng H, Wang Z, et al. Investigation on the misalignment of full ceramic ball bearing rotor system caused by varying gap in wide temperature ranges. Proceedings of the Institution of Mechanical Engineers, Part C: Journal of Mechanical Engineering Science, 2022. https://doi.org/10.1177/09544062221132184

[18] Wang P, Xu H, Yang Y, et al. Dynamic characteristics of ball bearing-coupling-rotor system with angular misalignment fault. Nonlinear Dynamics, 2022, 108(4): 3391-3415. https://doi.org/10.1007/s11071-022-07451-1

[19] Nan G, Yao J, Chen X, et al. Coupling dynamics of pedestal looseness and impact-rub for rotor system with nonlinear support. Advances in Mechanical Engineering, 2024, 16(1). https://doi.org/10.1177/16878132231222907

[20] Hou D, Qi H, Li D, et al. High-speed train wheel set bearing fault diagnosis and prognostics: Research on acoustic emission detection mechanism. Mechanical Systems and Signal Processing, 2022, 179. https://doi.org/10.1016/j.ymssp.2022.109325

[21] Li C, Qin Y, Wang Y, et al. Vibration analysis of deep groove ball bearings with local defect using a new displacement excitation function. Journal of Tribology, 2020, 142(12). https://doi.org/10.1115/1.4048163

[22] Bizarre L, Nonato F, Cavalca K L. Formulation of five degrees of freedom ball bearing model accounting for the nonlinear stiffness and damping of elastohydrodynamic point contacts. Mechanism and Machine Theory, 2018, 124: 179-196. https://doi.org/10.1016/j.mechmachtheory.2018.03.001

[23] Nan G, Zhang Y, Zhu Y, et al. Nonlinear dynamics of rotor system supported by bearing with waviness. Science Progress, 2020, 103(3). https://doi.org/10.1177/0036850420944092

[24] Deng H, Diao Y, Wu W, et al. A high-speed D-CART online fault diagnosis algorithm for rotor systems. Applied Intelligence, 2020, 50: 29-41. https://doi.org/10.1007/s10489-019-01516-2

[25] Ameid T, Ammar A, Talhaoui H, et al. An automatic rotor bar fault diagnosis using fuzzy logic and DWT-energy for backstepping control driven induction motor in low-speed operation. Soft Computing, 2023, 27(15): 10411-10426. https://doi.org/10.1007/s00500-023-08443-y

Submitted: 07.5.2024

Accepted: 08.10.2024

Assist. Prof. Zhongtang Huo
Dr. Jianqi Chen*
Dr. Lingjuan Hao
Dr. Jiansong Gao
Mechanical and Electrical College,
Handan University, Hanshan District,
Handan City, Hebei, China
*Corresponding author:
chenjianqi1106@163.com